

## STRONG MOTION PREDICTION ON ROCK SURFACE BY SUPERPOSED EVOLUTIONARY SPECTRA

Masata SUGITO<sup>1</sup>, Yoshinori FURUMOTO<sup>2</sup> And Takeshi SUGIYAMA<sup>3</sup>

### SUMMARY

Nonstationary strong motion prediction models are developed on the basis of rock surface strong motion dataset. Ground motion on rock surface with the shear wave velocity of 500–600 m/sec are dealt with. The strong motion dataset consists of 118 components of major Japanese accelerograms including the records from the 1995 Hyogoken-nambu Earthquake. The input motion at an engineering foundation level with the shear wave velocity of  $v_s = 500\text{--}600$  m/sec are estimated by the modified equivalent linearization technique in frequency domain which is called 'FDEL'. On the basis of the dataset, two types of prediction models are developed: the Model-I for given earthquake magnitude and hypo-central distance, and the Model-II for given fault parameters, such as fault length and width, seismic moment of fault, rupture pattern and rupture velocity, and propagation velocity of seismic waves. The Model-II incorporates the effect of fault size, successive fault rupture, and rupture direction, on characteristics of ground motion. In the Model-II, the evolutionary power spectrum from large earthquake is calculated by superposing those from unit event which corresponds to the earthquake of  $M=6.0$  in the Model-I. The ground motion simulation is performed by the Model-II for the fault model of the 1923 Great Kanto Earthquake. The effect of rupture velocity on simulated ground motion is demonstrated.

### INTRODUCTION

Simulation of earthquake ground motion at specific sites for given earthquake scale and source-to-site distance is a significant subject in earthquake engineering. Numerical calculation on the basis of theoretical approach for given simple fault parameters can simulate recorded ground motion successfully in relatively low frequency region such as  $f < 0.1$  Hz. In contrast, it is still difficult to simulate ground motion theoretically in middle and high frequency regions, since the ground motion in such frequency regions is strongly affected by detailed dynamic faulting parameters, irregularity of propagation path, and local soil structures. In Fig.1, for example, the acceleration Fourier spectra determined by the simple theoretical fault model are compared with that by the record obtained on hard ground surface during the 1968 Tokachi-oki Earthquake. For the numerical calculation, the fault parameters, such as the seismic moment, density, quality factor, and shear wave velocity of medium, corner frequency, and site-to-source distance, are used (McGuire and Hanks, 1980). It is observed that the Fourier spectra determined by given fault parameters are considerably less than that from the record in the frequency region of  $f > 1.0$  Hz.

In this paper a prediction model for strong ground motion on rock surface is developed on the basis of strong motion dataset which consists of 118 components of modified rock surface ground motion. The model incorporates the effect of direction of successive faulting relative to site using the superposing technique of evolutionary power spectra in time domain.

<sup>1</sup> Department of Civil Engineering, Gifu University, Gifu, Japan Email:sugito@cive.gifu-u.ac.jp

<sup>2</sup> Department of Civil Engineering, Gifu University, Gifu, Japan Email:furumoto@cive.gifu-u.ac.jp

<sup>3</sup> Electric Power Research & Development Center, Chubu Electric Power Company, Japan Email:sugiyama.takeshi2@chuden.co.jp

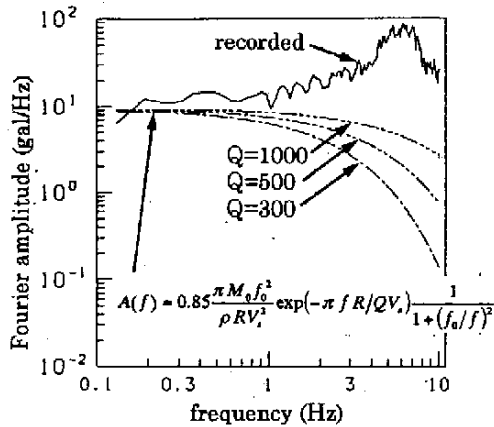


Fig.1 Acceleration Fourier amplitudes for theoretical fault model and strong motion record.

Table 1 Classification of strong motion dataset.

contents	No. of records	No. of sites
A: records on soil ground surface	106	21
B: records at underground bed rock	6	3
C: records on rock surface	6	1

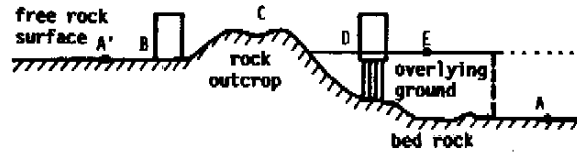


Fig.2 Illustration of bed rock and free rock surface.

**STRONG MOTION DATASET**

**Definition of Rock Surface**

For engineering purposes rock surface with the shear wave velocity about  $v_s=700$  m/sec has been frequently dealt with (Hisada, et. al., 1978). It is well known that the ground motion is strongly effected by local soil condition, such as soil structure from ground surface to the basement with the shear wave velocity level like  $v_s=500\sim 600$  m/sec. Therefore, the simulation model in the present paper is developed for the ground motion on the stiff ground level with the shear wave velocity of  $v_s=500\sim 600$  m/sec. Consequently, the ground motion on deposit site can be easily obtained by the response analysis of sub-surface ground for given input motion and soil structure model. In this paper, this stiff free ground level is called as "free rock surface". Figure 2 shows a schematic illustration for free rock surface and other related site conditions. Point A represents an imaginary case where overlying deposits are removed, and Point A' is an actual case for free rock surface. For other cases ground motions can be used after some appropriate modifications such as response analysis of soil layers (E), of irregular ground (C), and of soil structure interactions (B,D).

**Estimation of Free Rock Surface Ground Motion**

Strong motion data used in this paper consist of 118 components of acceleration time histories which have been obtained at 25 stations during 37 Japanese earthquakes. Table 1 shows the items of the data which are classified into 3 groups. The group A represents the modified acceleration time histories on free rock surface which have been estimated from the records obtained on soil deposit sites. The group B represents the modified free rock surface motion which have been estimated from the records obtained at underground seismographs in borehole observation sites. The group C represents the records obtained on free rock surface stations. In the calculation of free rock surface motion in the group A and B, the modified equivalent linearization method for the response analysis of layered ground, which is called FDEL (Sugito, et. al., 1994), has been applied.

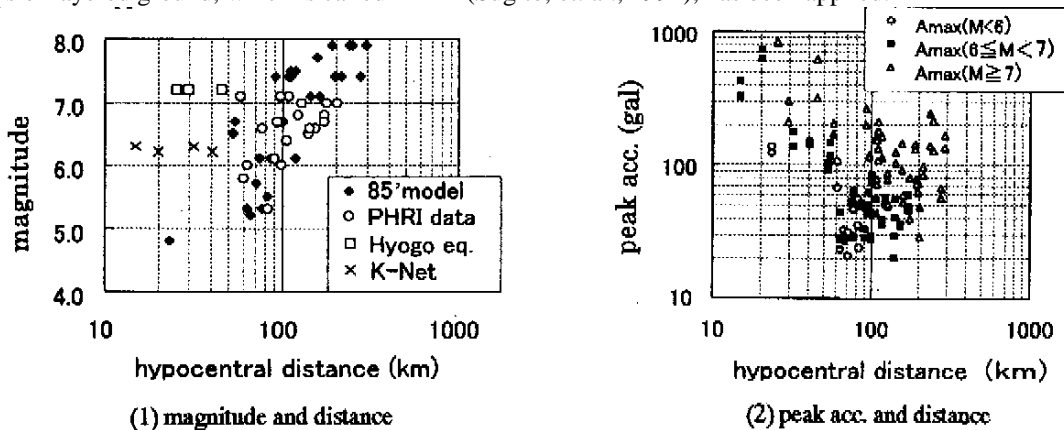


Fig.3 Scattergram of magnitude, peak acceleration, and hypo-central distance for the strong motion dataset.

Figure 3 shows the scattergram of magnitude and hypo-central distance, and the relation between peak acceleration and hypo-central distance of the dataset. In Fig.3(1), 85' model represents the data which has been used in the previous paper (Sugito, et.al., 1985). 'PHRI data' represents the data obtained by the Port and Harbor Research Institute, Ministry of Transport, during from 1986 to 1993. 'Hyogo eq.' represents the data obtained during the 1995 Hyogo-ken nambu Earthquake. 'K-net' represents the data obtained by the National Research Institute for Earth Science and Disaster Prevention. As shown in Fig.3(1) much more data for near fault region are included compared with those in 85-model.

## PREDICTION MODEL FOR GIVEN MAGNITUDE AND DISTANCE (MODEL-I)

### Simulation of ground motion by evolutionary process

Based on the 118 components of modified rock surface motion explained above, the earthquake motion prediction model for given earthquake magnitude and hypo-central distance has been proposed. The procedure to complete the model is same as that developed in the previous study (Sugito and Kameda, 1985).

Earthquake acceleration with nonstationary frequency content can be represented by

$$x(t) = \sum_{k=1}^m \sqrt{4\pi \cdot G_x(t, 2\pi f_k) \Delta f} \cdot \cos(2\pi f_k t + \phi_k) \quad (1)$$

in which  $\sqrt{G_x(t, 2\pi f_k)}$  = evolutionary power spectrum (Kameda, 1975) for time  $t$  and frequency  $f_k$ ,  $\phi_k$  = independent random phase angles distributed over  $0 \sim 2\pi$ , and  $m$  = number of superposed harmonic components. The upper and lower boundary frequencies,  $f_u, f_l$ , are fixed as  $f_u = 10.03$  Hz,  $f_l = 0.13$  Hz, and also  $m$  and  $\Delta f$  are fixed as  $m = 166$  and  $\Delta f = 0.06$  Hz. The following time-varying function is adopted for the model of  $\sqrt{G_x(t, 2\pi f)}$ .

$$\sqrt{G_x(t, 2\pi f)} = \alpha_m(f) \frac{t - t_s(f)}{t_p(f)} \exp\left(1 - \frac{t - t_s(f)}{t_p(f)}\right) \quad ; t > t_s(f) \quad (2)$$

in which  $t_s(f)$ ,  $t_p(f)$  = starting time and duration parameter, respectively, and  $\alpha_m(f)$  = intensity parameter which represents the peak value of  $\sqrt{G_x(t, 2\pi f)}$ . These parameters have been determined relative to recorded acceleration time histories (Kameda, et. al., 1980). Figure 4 shows example of recorded and modeled evolutionary spectra.

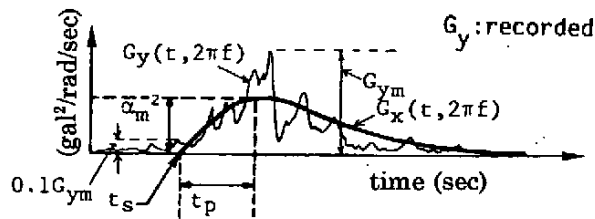


Fig.4 Recorded and simulated evolutionary power spectra.

Table 2 Estimation formulas for model parameters and correction factor  $\beta(f, M_0)$ .

$\log \alpha_m(f) = B_0(f) + B_1(f) \cdot M - B_2(f) \cdot \log(R)$	(3)
$B_0(f) = -0.657 + 1.637 \cdot \log f - 1.642 \cdot (\log f)^2$	(4)
$B_1(f) = 0.563 - 0.208 \cdot \log f + 0.0198 \cdot (\log f)^2$	
$B_2(f) = -1.335 - 0.115 \cdot \log f - 0.443 \cdot (\log f)^2$	
$\log t_p(f) = P_0(f) + P_1(f) \cdot M - P_2(f) \cdot \log(R)$	(5)
$P_0(f) = -0.808 - 0.929 \cdot \log f$	(6)
$P_1(f) = 0.123 + 0.134 \cdot \log f$	
$P_2(f) = 0.357 - 0.083 \cdot \log f$	
$i_s(f) = t_s(f) - t_m = S_0(f) + S_1(f) \cdot R$	(7)
$S_0(f) = 0.0$ (fixed)	(8)
$S_1(f) = (0.863 - 0.509 \cdot \log f - 1.141 \cdot (\log f)^2) \times 10^{-2}$	
$\log \beta_0(f, M_0) = d_0(f) + d_1(f) \cdot \log(M_0)$	(13)
$d_0(f) = -0.449 + 0.641 \cdot \log f + 0.178 \cdot (\log f)^2$	(14)
$d_1(f) = 0.0157 - 0.0306 \cdot \log f$	

**Prediction model for given magnitude and distance**

The regression equations listed in Table 2 are used for the model parameters to establish the prediction model for given magnitude and distance. In Eq.(7),  $t_m$  represents the average value of  $t_s(f)$  over the frequency range considered herein for each individual component. The parameter  $t_s'(f)$ , which represents the residual time from  $t_m$ , is necessary since the recorded accelerograms used for statistical analysis have been obtained only on relative reference times.

The coefficients for the model parameters in Eqs.(3), (5), and (7) have some typical inclination on the frequency axis, they were modeled as a function of frequency using the least square method. The modification of the coefficients have been discussed in detail in the previous study (Goto, et. al., 1984). The formulas for the modeled coefficients to be used in Eqs.(3), (5), and (7) are listed in Table 2.

For given earthquake magnitude  $M$  and hypo-central distance  $R$ , the model parameters,  $\alpha_m(f)$ ,  $t_p(f)$ , and  $t_s(f)$ , are obtained by using the Eqs.(3)~(8), and the evolutionary power spectra are obtained by Eq.(2). Finally, acceleration time history for given  $M$  and  $R$  are simulated by Eq.(1). Figure 5 shows the typical examples of simulated rock surface strong motion time histories for the case of (1)  $M = 7.5, R = 70$  km, and (2)  $M = 6.5, R = 25$  km. It is observed that the peak ground motions do not differ so much, however, the duration is much longer for the case (1) because of the larger magnitude and longer distance.

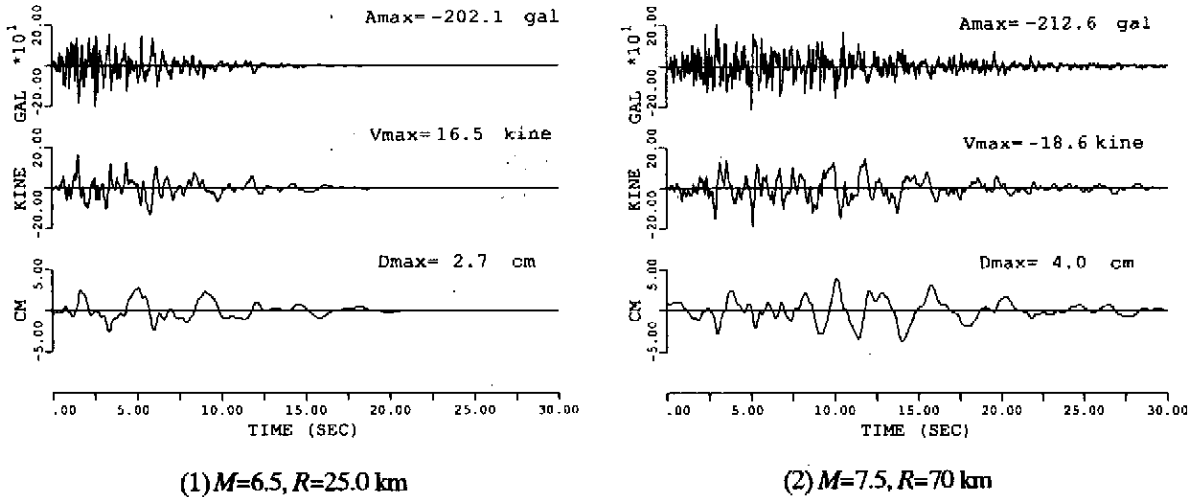


**Fig.5 Simulated strong ground motion by Model-I.**

**PREDICTION MODEL FOR GIVEN FAULT PARAMETERS (MODEL-II)**

**Superposition of evolutionary power spectra from small earthquake event**

It is known that the past strong motion records obtained from great earthquakes show the effect of rupture direction relative to sites and geometrical condition between sites and fault on ground motion intensities and their duration. In the case that these physical fault parameters in addition to the earthquake magnitude are given for the ground motion prediction, to incorporate these parameters effectively is important in the engineering subjects. Herein the basic prediction model obtained in the Chapter 3 is extended into the model which incorporates a size of fault, fault rupture direction and its velocity, and seismic moment as a parameter of earthquake scale.

Figure 6 gives general concept of the model. A fault is divided into a number of small events which correspond to the unit event of magnitude  $M=6.0$  in the Model-I. In this extended model, the arriving time lag resulted from rupture on the fault and difference of propagation distance of ground motions for each individual unit event are considered. Consequently, the evolutionary power spectra for great earthquakes are given from the superposition of those from each unit event on the time domain. Figure 7 shows the schematic illustration of the superposition of evolutionary spectra

### Number of superposition, $N_G$ , scaled for seismic moment

The number of superposition,  $N_G$ , of evolutionary spectra is defined. The parameter,  $N_G$ , represents the number of small unit events on a specific great fault. The following procedure has been performed to obtain the superposition parameter. The magnification factor,  $c(f)$ , defined by Eq.(9) can be used for amplification value of evolutionary power spectrum.

$$c(f) = \int_0^{t_0} \sqrt{G_x(t, 2\pi f)} dt / \int_0^{t_0} \sqrt{G_x^*(t, 2\pi f)} dt \quad (9)$$

where  $G_x(t, 2\pi f)$  = simulated evolutionary spectrum for the specific data,  $G_x^*(t, 2\pi f)$  = evolutionary spectrum given from the Model-I which corresponds to the earthquake magnitude  $M=6.0$  and the 'same hypo-central distance' of the specific data, and  $t_0$  = duration of the record. The number of superposition,  $N_G$ , the average of the magnification factor,  $c(f)$ , along the logarithmic frequency axis is defined as,

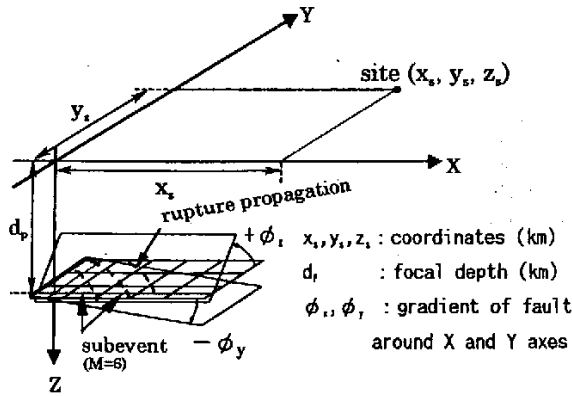


Fig.6 Fault modeling with multiple fault rupture.

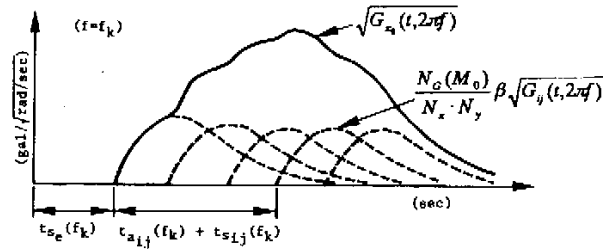


Fig.7 Superposed evolutionary power spectra.

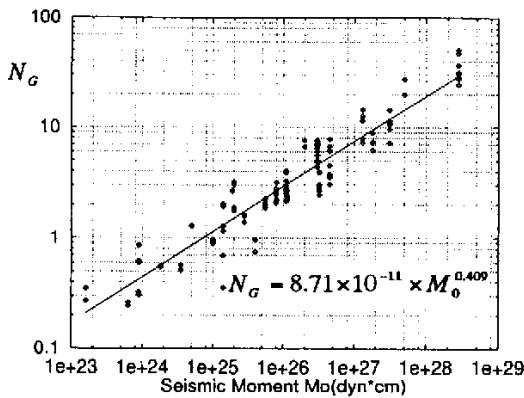


Fig.8 Relation between number of superposition  $N_G$  and seismic moment.

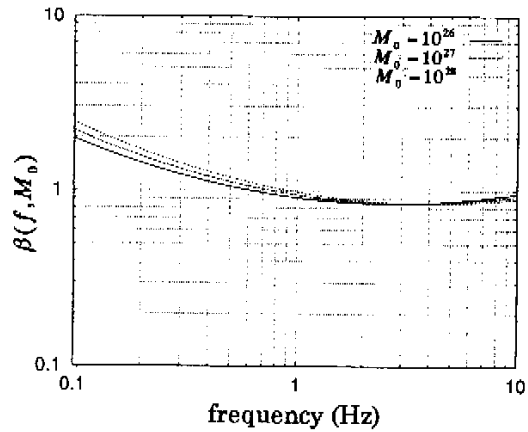


Fig.9 Variation of correction factor  $\beta(f, M_0)$  for seismic moment.

$$N_G = \int_{\log f_1}^{\log f_2} c(f) d(\log f) / (\log f_2 - \log f_1) \quad (10)$$

where the lower and upper frequencies  $f_1, f_2$  are fixed as  $f_1 = 0.13$  Hz and  $f_2 = 10.03$  Hz. The parameter,  $N_G$ , has been obtained for 118 components of acceleration time histories. Figure 8 shows the relation between the parameter,  $N_G$ , and the seismic moment,  $M_0$ . The parameter,  $N_G$ , has been scaled for  $M_0$ , and the following relation has been obtained.

$$N_G = 8.71 \times 10^{-11} \times M_0^{0.409} \quad (11)$$

In Eq.(11) the value  $M_0$  which gives  $N_G = 1.0$  is obtained as  $M_0 = 7.13 \times 10^{24}$  dyne cm. This value nearly coincides with  $M_0 = 7.76 \times 10^{24}$  for  $M_s = 6.0$  which is obtained in the relation between  $M_0$  and surface magnitude,  $M_s$  (Geller, 1976).

The superposed evolutionary spectra for great earthquake is given by

$$\sqrt{G_{x_0}(t, 2\pi f)} = \frac{N_G(M_0)}{N_x \cdot N_y} \beta(f, M_0) \sum_{i=1}^{N_x} \sum_{j=1}^{N_y} \sqrt{G_{ij}(t, 2\pi f)} \quad (12)$$

where  $G_{ij}$  = evolutionary spectrum for each unit event  $e_{ij}$  corresponding to the earthquake magnitude  $M=6.0$  and hypo-central distance  $R_{ij}$  in the Model-I, and the suffix,  $i$  and  $j$ , represent the position of each event on the fault.  $N_x$  and  $N_y$  represent the number of unit event in the direction of fault width and length. The number of superposition,  $N_G$ , is generally not an integral number, therefore the term  $N_x \times N_y$  is necessary to keep the superposed power correctly. Further the correction factor  $\beta(f, M_0)$  in Eq.(12) is incorporated for superposing of each frequency component, since the number of superposing of evolutionary spectra depends on the frequency. This correction factor,  $\beta(f, M_0)$ , has been obtained from the regression analysis of the parameter,  $c(f)$ , defined by Eq.(9) on seismic moment. The estimation formula for the correction factor,  $\beta(f, M_0)$ , is given in Table 2. Figure 9 shows the value of the factor,  $\beta(f, M_0)$ , for three given seismic moments. It is observed that the correction factor for the superposition of evolutionary spectra along the frequency axis does not depend on the seismic moment, and it is larger than 1.0 for the frequency range,  $f < 1.0$  Hz, and is smaller than 1.0 for the frequency range,  $f > 1.0$  Hz.

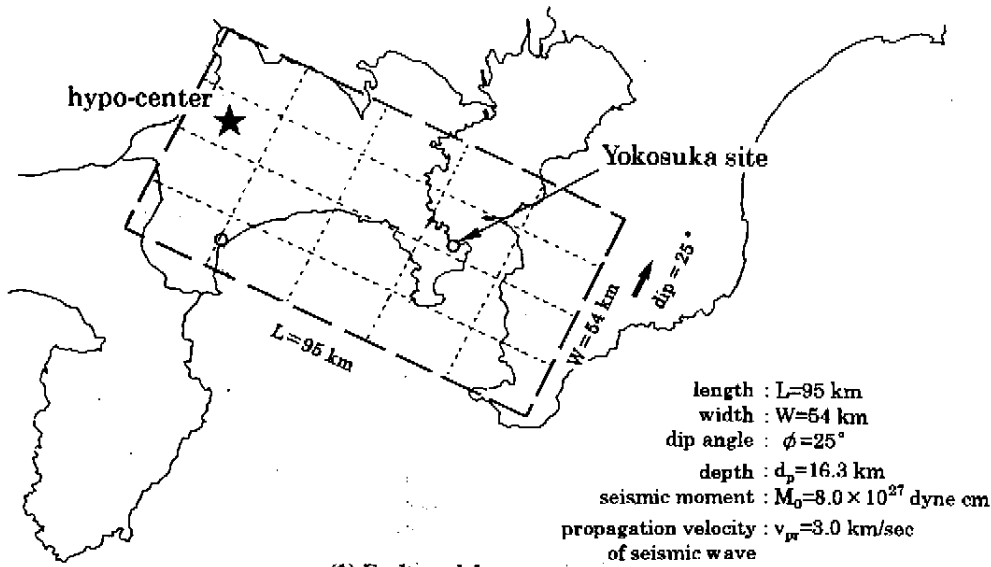
### Procedure of simulation by the Model-II

The procedure of the ground motion simulation by the Model-II is as follows.

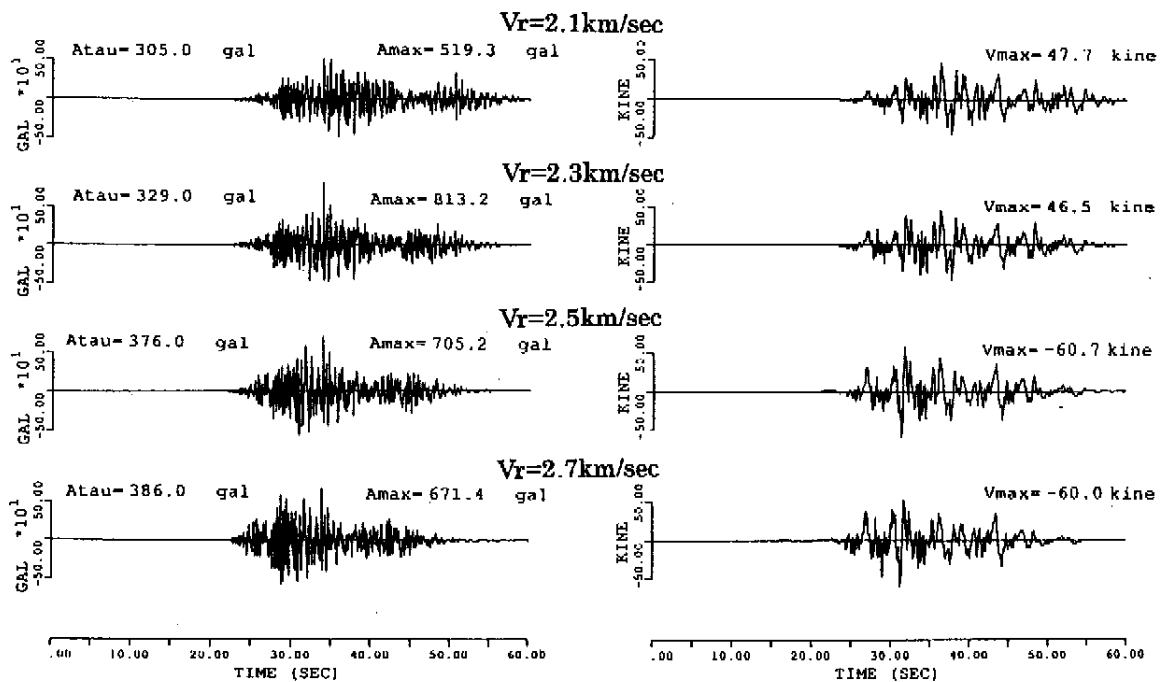
- (1) Calculate the number of superposition,  $N_G$ , for given seismic moment,  $M_0$ , by Eq.(11), and find the integral numbers,  $N_x$  and  $N_y$ , by which the given fault can be divided properly according to the fault dimension.
- (2) Calculate the hypo-central distance,  $R_{ij}$ , and mean arrival time lag,  $t_{a_{ij}}$ , in Fig.7 of seismic motion for each unit event considering the fault dimension, rupture velocity, and propagation velocity of seismic waves, as well as the geometrical condition between a specific site and a fault.
- (3) Calculate the evolutionary spectra,  $G_{ij}$ , for each distance,  $R_{ij}$ , and  $M=6.0$  using the Model-I, and superpose the evolutionary power spectra,  $G_{x_0}$ , considering the arrival time lag of each unit event.
- (4) Generate the ground motion time history by Eq.(1) substituting  $G_{x_0}$  to  $G_x$ .

### Example of ground motion simulation by Model-II

An example for ground motion simulation for given fault parameters is shown in Fig.10. Figure 10(1) shows the fault model for the 1923 Great Kanto Earthquake (partly after Matsu'ura, et. al., 1980) and the location of simulation site in Yokosuka City. The length and the width of the fault is given as  $L=95$  km and  $W=54$  km, respectively. The seismic moment of the fault is given as  $M_0=8.0 \times 10^{27}$  dyne cm. The depth of the hypo-center is given as  $d_p=16.3$  km. The ground motion simulation has been performed for 4 cases of the rupture velocity,  $v_r$ , as  $v_r=2.1, 2.3, 2.5,$  and  $2.7$  km/sec, respectively. The propagation velocity of seismic waves from source to site is fixed as  $v_{pr}=3.0$  km/sec. Figure 10(2) shows the simulated acceleration and velocity time histories for 4 cases of rupture velocity. The parameter,  $A_{tau}$ , in Fig.10(2) represents the equivalent peak acceleration calculated from the filtered acceleration time history for determination of the JMA seismic intensity. As shown in Fig.10(2), the equivalent peak acceleration increases with increase in the rupture velocity, since the power of ground motion is generally concentrated on the time axis in the case that the rupture velocity is close to the propagation velocity of seismic waves. In contrast, the peak acceleration fluctuates randomly not depending on the rupture velocity.



(1) Fault model



(2) simulated acceleration and velocity time histories

Fig.10 Simulated strong ground motion by Model-II for the 1923 Great Kanto Earthquake.

### CONCLUSIONS

- (1) The strong motion dataset was arranged, which consists of 118 components of major Japanese accelerograms including the records from the 1995 Hyogoken-nambu Earthquake. The input motion at an engineering foundation level with the shear wave velocity of  $v_s = 500 \sim 600$  m/sec were estimated by the modified frequency domain analysis, FDEL.
- (2) The nonstationary earthquake motion prediction model on free rock surface (Model-I) for given magnitude and hypo-central distance was developed on the basis of the rock surface strong motion dataset.
- (3) The Model-I was extended to the prediction model for the case that more detailed fault parameters are given.

The parameters used in the Model-II are the seismic moment, size and geometrical condition of the fault, and rupture velocity and its direction on the fault. The Model-II incorporates the effect of fault size, successive fault rupture, and rupture direction, on characteristics of ground motion. In the Model-II, the evolutionary power spectrum from a large earthquake is calculated by superposing those from unit events which correspond to the earthquake of  $M=6.0$  in the Model-I.

- (4) The ground motion was simulated using the Model-II for the fault model of the Great Kanto Earthquake. The dependence of the peak ground motion parameters, such as a peak acceleration, peak velocity, and the equivalent peak acceleration used for the evaluation of the JMA seismic intensity, on the rupture velocity of faulting were demonstrated.

### ACKNOWLEDGEMENT

The authors would like to express their deep appreciation to Mr. M. Horagai of Taisei Construction Company (formerly a Graduate student at Gifu University) for his help on the development of the rock surface strong motion dataset. This study was partly supported by the Association for Development of Earthquake Prediction and Japan Society for the Promotion of Science, Grant-in-aid for Scientific Research (No.07650543).

### REFERENCES

- Goto, H., Sugito, M., Kameda, H., Saito, H., and Ohtaki, T. (1984), "Prediction of Nonstationary Earthquake Motions for Moderate and Great Earthquakes on Rock Surface," *Annuals, Disaster Prevention Research Institute*, Kyoto University, Vol.27, B-2, pp.19-48.
- Hisada, T., Ohsaki, Y., Watabe, M., and Ohta, T. (1978), "Design Spectra for Stiff Structures on Rock," *2<sup>nd</sup> International Earthquake Microzonation Conference*, Vol.III, pp.1178-1198.
- Kameda, H. (1975), "Evolutionary Spectra of Seismogram by Multifilter," *Journal of Engineering Mechanics Division, ASCE*, Vol.101, pp.787-801.
- Matsu'ura, M., Iwasaki, T., Suzuki, Y., and Sato, R. (1980), "Static and Dynamic Study on Faulting Mechanism of the 1923 Kanto Earthquake," *J. Phys. Earth*, **28**, pp.119-143.
- McGuire, R.K., and Hanks, T.C. (1980), "Rms Accelerations and Spectral Amplitudes of Ground Motion During the San Fernando, California Earthquake", *BSSA*, Vol.70, pp.1907-1919.
- Sugito, M. and Kameda, H. (1985) "Prediction of Nonstationary Earthquake Motions on Rock Surface," *Proc. of JSCE Structural Eng./Earthquake Eng.*, Vol.2, No.2 (No.362) pp.149-159.
- Sugito, M. (1995), "Frequency-dependent Equivalent Strain for Earthquake Response Analysis of Soft Ground," *Proc. of IS-Tokyo, '95, The First International Conference on Earthquake Geotechnical Engineering*, Tokyo, pp.655-660.